ACS OMEGA

http://pubs.acs.org/journal/acsodf

Article

In Silico Tuning of the Pore Surface Functionality in Al-MOFs for Trace CH_3I Capture

Xiaoyu Wu, Linjiang Chen,* Eric Jean Amigues, Ruiyao Wang, Zhongfu Pang, and Lifeng Ding*

Cite This: *ACS Omega* 2021, 6, 18169−18177

Read Online

ACCESS | Metrics & More | Article Recommendations | Supporting Information

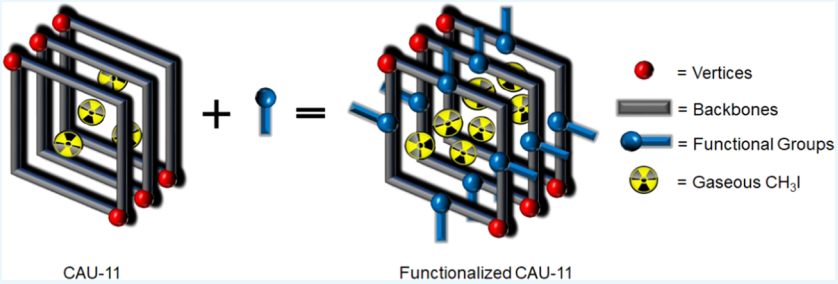

ABSTRACT: Aluminum (Al)-based metal−organic frameworks (MOFs) have been shown to have good stability toward γ irradiation, making them promising candidates for durable adsorbents for capturing volatile radioactive nuclides. In this work, we studied a series of existing Al-MOFs to capture trace radioactive organic iodide (ROI) from a gas composition (100 ppm CH_3I, 400 ppm CO_2, 21% O_2, and 78% N_2) resembling the off-gas composition from reprocessing the used nuclear fuel using Grand canonical Monte Carlo (GCMC) simulations and density functional theory (DFT) calculations. Based on the results and understanding established from studying the existing Al-MOFs, we proceed by functionalizing the top-performing CAU-11 with different functional groups to propose better MOFs for ROI capture. Our study suggests that extraordinary ROI adsorption and separation capability could be realized by $-SO_3H$ functionalization in CAU-11. It was mainly owing to the joint effect of the enhanced pore surface polarity arising from $-SO_3H$ functionalization and the μ-OH group of CAU-11.

INTRODUCTION

Nuclear energy is promising to be one of the leading emission-free energy source to power the global economy.[1,2] During reprocessing the used nuclear fuel or tackling nuclear accidents,[3] the removal of the harmful volatile radioactive nuclides, ^{129}I, ^{131}I with their molecular forms iodine (I_2), and radioactive organic iodides (ROI), is essential to ensure the safe use of the nuclear energy.[4] Compared with iodine, CH_3I, which is the main kind of the ROI species, is known to be much more difficult to be separated and immobilized because of its comparatively inert chemical reactivity.[5] Existing methods for ROI retention and separation based on adsorption include immobilizing gaseous iodine onto AgZ,[6] activated charcoals,[7] and amine-impregnated activated carbon.[8,9] However, high regeneration costs and poor separation efficiency have limited these adsorbents from having wide applications.[10]

As a novel class of functional porous crystalline solids that are assembled using "Molecular Lego"-like organic/inorganic blocks, metal−organic frameworks (MOFs) have been receiving growing interest for ROI capture in the past few years. Unlike conventional porous adsorbents, MOFs feature their tunable pore geometry, precise surface functionality control, large surface areas, and the ease for postsynthetic functionalization, which render them as a new generation of functional materials for adsorption and separation applications. Recently, Chebbi et al.[11] investigated a series of MOFs for CH_3I capture at 35 °C, in which HKUST-1(Cu) had the highest saturated CH_3I uptake (425 mg/g). Li et al.[12,13] suggested that a total CH_3I uptake of 80 wt % could be reached under 150 °C by *N*,*N*′-dimethyl ethylenediamine (DMEDA)-grafted MIL-101(Cr) due to the strong ionic coupling of CH_3I with tertiary nitrogen of an amine group forming ionic $(R_3N{-}CH_3)^+I^-$. Lan et al.[14] computationally screened 187 covalent organic frameworks COFs (which are MOFs' analogue but the main composition is light element linked by covalent bonds) for I_2 and CH_3I capture. They found that 3D-Py-COFs with a larger accessible surface area or a void fraction have the best I_2 uptake and COF-103 with a pore size of 9 Å is identified as the best-performing material for CH_3I capture, respectively. The durability of MOFs has always been a concern when MOFs are employed in practical applications.[15,16]

Received: April 19, 2021
Accepted: June 24, 2021
Published: July 12, 2021

https://doi.org/10.1021/acsomega.1c02072
ACS Omega 2021, 6, 18169−18177

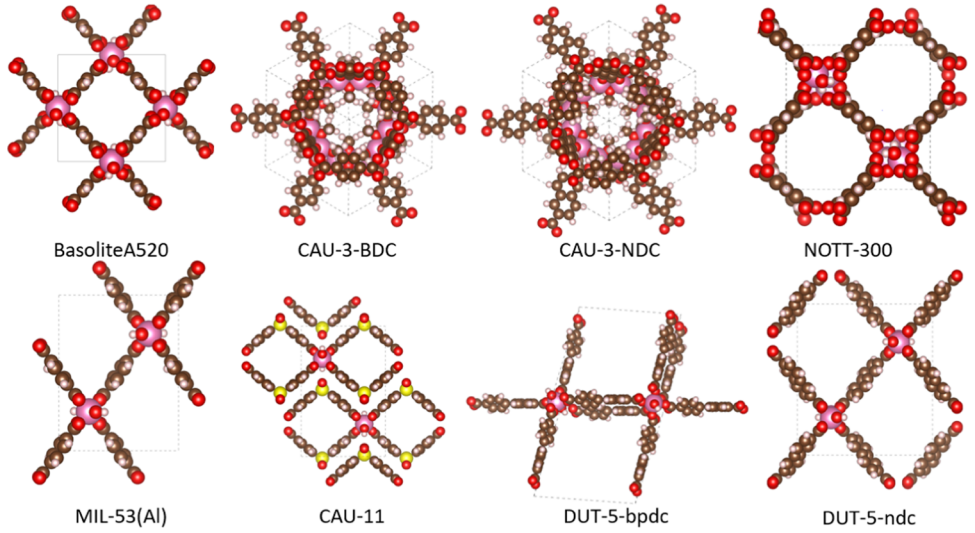

Figure 1. Space-filling model of the selected Al-MOFs in this work (color scheme: Al, pink; C, brown; O, red; and H, white. The model of CAU-8-ODB can be found in the Supporting Information (Figure S1)).

Table 1. Selected Al-MOF Properties and Separation Performance under Simulated Conditions

MOF	ligand molecules	uptake (cm^3/g)	selectivity	LCD[a] (Å)	SA_{sim}[b] (m^2/g)	SA_{exp} (m^2/g)	$V_{p\text{-}sim}$[c] (cm^3/g)	$V_{p\text{-}exp}$ (cm^3/g)
BasoliteA520[18]	FA[d]	2.24	8.18×10^3	5.82	1174.66	1025	0.56	0.47
CAU-3-BDC[19]	H_2BDC[e]	0.07	4.06×10^2	11.07	2389.16	1920	0.88	0.64
MIL-53[24]	H_2BDC	0.52	2.19×10^3	6.97	1410.96	1140	0.61	0.68
CAU-3-NDC[19]	H_2NDC[f]	0.04	2.02×10^2	13.81	3129.4	2750	1.17	0.95
CAU-11[20]	H_2SDBA[g]	11.18	6.64×10^4	5.89	469.78	350	0.31	0.17
DUT-5-bpdc[21]	H_2bpdc[h]	0.04	1.93×10^2	11.33	2376.25	2335	1.08	0.81
DUT-5-ndc[21]	H_2NDC	0.09	4.41×10^2	8.90	2067.21	1996	0.83	0.68
NOTT-300[22]	H_4L[i]	1.19	3.75×10^3	5.72	1326.7	1370	0.54	0.38
CAU-8-ODB[23]	H_2ODB[j]	0.36	1.91×10^3	6.74	1401.78	1004	0.67	0.47

[a]Largest cavity diameter. [b]Geometric surface area. [c]Pore volume. [d]Fumaric acid. [e]Terephthalic acid. [f]1,4-Naphthalenedicarboxylic acid. [g]4,4′-Sulfonyldibenzoic acid. [h]4,4′-Biphenyldicarboxylic acid. [i]Biphenyl-3,3′,5,5′-tetracarboxylic acid. [j]4,4′-Oxydibenzoic acid.

Volkringer et al. performed a study of the structural stability of a series of MOFs under γ irradiation, where Al-based MOFs were demonstrated to be able to remain intact under a γ irradiation with doses up to 1.75 mGy, whereas the other tested transition-metal-based MOF materials, such as HKUST-1(Cu) and UiO-66(Zr), were destructed under such irradiation. The radiation stability of the Al-based MOFs was attributed to the smaller γ-ray absorption cross section of aluminum (2.5 barns per atom), compared to those of the transition metals, copper, zinc, and zirconium (>5.3 barns per atom); a smaller cross section implies a lower γ ray absorption and hence higher robustness of the MOF under γ irradiation.[17] Inspired by Volkringer et al.'s study, we envisage that other Al-based MOFs might also exhibit a high resistance to γ irradiation, which is a desirable property of the adsorbent materials for capturing volatile ROIs in an irradiation environment. However, we did not attempt any MOF synthesis or stability test under γ irradiation in this study, but we offer our predictions as experimental targets for the future.

Herein, we investigated a series of Al-based MOFs: BasoliteA520,[18] CAU-3-BDC,[19] CAU-3-NDC,[19] CAU-11,[20] DUT-5-bpdc,[21] DUT-5-ndc,[21] NOTT-300,[22] and CAU-8-ODB[23] for capturing trace CH_3I resembling the used nuclear fuel reprocessing conditions (Figure 1). All of the selected Al-MOFs were previously reported to have good thermal and chemical stability. Six out of the total nine Al-MOFs structures feature 1D metal-oxide chain except for 2D MOF CAU-8-ODB and 3D MOF CAU-3-NDC and CAU-3-BDC, which possess a similar rhombohedral system while differ in secondary building edges (BDC^{2-} and NDC^{2-}, respectively). Unlike other Al-MOFs, which contain a μ-OH group, O-CH_3I in CAU-3 series bridges the Al^{3+} vertices. GCMC simulations and DFT calculations were employed to study the adsorption and separation performance of CH_3I in the MOFs. Our modeling results suggested that CAU-11 possessed both the top-performing CH_3I adsorption capacity and selectivity. Based on the experimental fact that CAU-11 has been successfully functionalized through a postsynthetic approach without harming the parent framework,[25] we propose a series of hypothetic CAU-11 derivatives (namely, CAU-11-X) by grafting a series of functional groups on to the SDBA linker of CAU-11 to further promote the separation performance of trace CH_3I under a realistic condition. This study of fine-tuning the surface functionalities and pore geometry will aid in the novel design of low-cost and stable materials for effective ROI capture for industrial applications. To our best knowledge, this is the first systematic investigation of trace CH_3I capture using Al-based radiation-resistant MOFs.

https://doi.org/10.1021/acsomega.1c02072
ACS Omega 2021, 6, 18169−18177

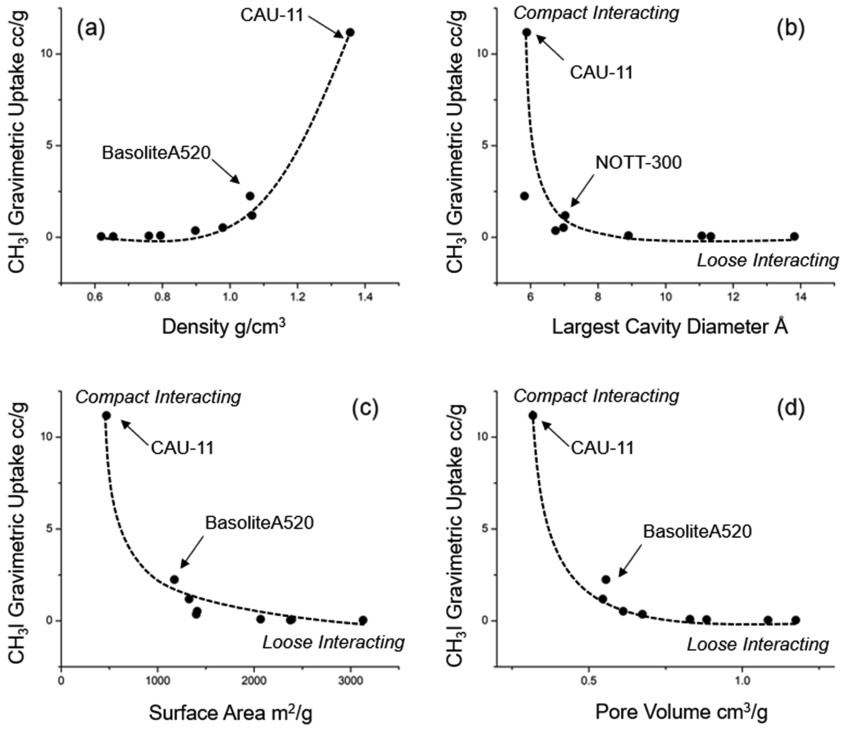

Figure 2. Competitive CH_3I uptake structure−property relationship of the selected Al-MOFs as a function of (a) framework density, (b) largest cavity diameter Å, (c) surface area m^2/g, and (d) pore volume cm^3/g (dashed line represents the fitting curve of the scatter trend).

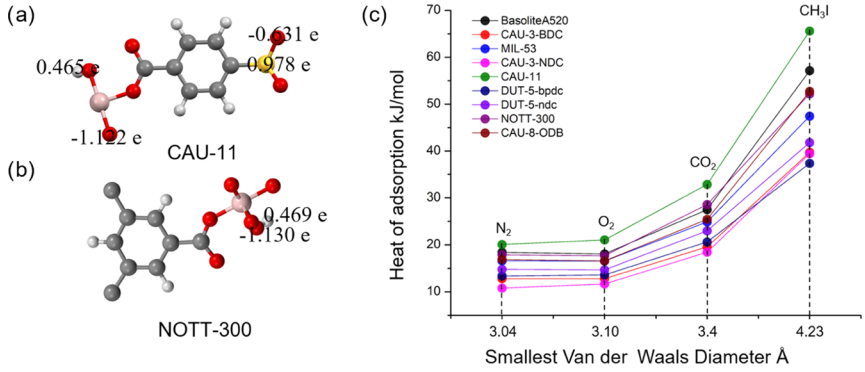

Figure 3. (a, b) Schematic illustrations of the asymmetric unit of CAU-11 and NOTT-300 with the atomic point charge (color scheme: C, gray; H, white; O, red; Al, pink; and S, gold). (c) Isosteric heat of adsorption of the adsorbates at infinite dilution in the Al-MOFs.

RESULTS AND DISCUSSION

Table 1 presents the geometric properties together with separation performance of the selected Al-MOFs. We noted that the theoretically calculated surface area and porosity of Al-MOFs are slightly higher than those reported from experiments. This could be attributed to imperfect crystalline or incomplete activation during MOF synthesis.[25] With the abundant presence of CO_2, O_2, and N_2, the adsorption of dilute 100 ppm CH_3I in most of the selected MOFs has been difficult due to the competing nature of the other gas molecules against CH_3I. Nevertheless, there are a few well-performing MOFs with high CH_3I uptake, which possess relatively narrow pore channels. CAU-11, BasoliteA520, and NOTT-300, which possess relatively small largest cavity diameters (LCD) (5.89, 5.82, and 5.72 Å, respectively) enjoy high selective capture toward CH_3I (11.18, 2.24, and 1.19 cm^3/g, respectively). Such adsorption behavior that the separation performance could be enhanced by tuned pore size was also observed in studies of acid gas removal[26] and purification of natural gas using MOFs.[27]

To further reveal the correlation between MOF characteristics and the CH_3I separation capability, structure−property relationships were mapped for the selected nine Al-MOFs; as shown in Figure 2a, the CH_3I gravimetric uptake increases as density increases. However, a nonlinear correlation could be observed. Figure 2b−d shows that there is a sharp drop of CH_3I uptake when LCD, the surface area, and the pore volume of the MOFs are increased to around 6.5 Å, 1000 m^2/g, and 0.5 cm^3/g, respectively. Above all, extraordinary CH_3I capture performance (11.18 cm^3/g uptake and 6.64×10^4 selectivity) could be found in CAU-11 owing to compact interaction with CH_3I provided by a constricted porosity (surface area: 469.78 m^2/g and pore volume: 0.31 cm^3/g), followed by BasoliteA520 (surface area: 469.78 m^2/g and pore volume: 0.31 cm^3/g) and NOTT-300 (surface area: 469.78 m^2/g and pore volume: 0.31 cm^3/g).

https://doi.org/10.1021/acsomega.1c02072
ACS Omega 2021, 6, 18169−18177

Figure 3a presents the asymmetric edge unit of CAU-11, which forms the lozenge-shaped narrow channel geometry. Interconnected by an SDBA linker, Al^{3+} vertices were bridged through μ-OH groups.[25] Compared with NOTT-300 (Figure 3b) where only the μ-OH group contributes to an electrostatic field, the $-SO_2$ vertex of the SDBA ligand bridging two phenyl rings along with the μ-OH group also provides a polarized channel surface enhancing the electrostatic potential field. As indicated from the DDEC calculated atomic charges on the asymmetric unit of CAU-11 (Figure 3a), the sulfur atom formulating the V shape of the SDBA linker possess an atomic charge of 0.978e while the two neighboring oxygen atoms are charged around −0.631e. The hydrogen and oxygen atoms of the μ-OH group possess point charges of 0.465e and −1.122e, respectively. With the aid of 1-D narrow pore channels, the polarized pore surface provides the overlapped electrostatic interaction with CH_3I to enhance its uptake in CAU-11. As shown in Figure 3c, the isosteric heat of CH_3I in CAU-11 outperforms all other selected MOFs. Such tuned polarity of the channel surface in MOFs was studied to play vital roles in CO_2 storage and capture.[28,29]

As shown in Figure 4a, the phenol rings of SDBA ligands in CAU-11 have good coverage of the pore surface in CAU-11,

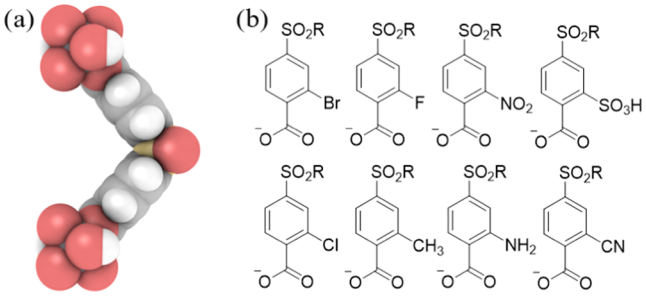

Figure 4. (a) Space-filling model of the SDBA linker. (b) Asymmetric unit of SDBA grafted by different functional group designed in this work (SO_2R refers to the other symmetric part of the SDBA-X ligand, X = functional group; CH_3I-inaccessible CAU-11-X were excluded).

which are the least polarized part of the ligands. We further grafted eight different types of functional groups in silico varying between polarities and size onto a phenol ring of the SDBA ligand to study to effect of pore size and tuned functionality onto the selective adsorption nature toward trace CH_3I. Potential synthetic routes for the grafted ligands (Figure 4b) are proposed in Section S10 of the Supporting Information. The $-SO_3H$-functionalized ligand, diphenylsulfone-3,3′-disulfo-4,4′-dicarboxylate, has been synthesized and used to construct MOFs before.[30] More generally, diarylsulfones show good versatility in incorporating chemical functionalities.[31] However, we envisage that some syntheses might be elaborate and challenging.

The hypothetical structures with grafting modification were optimized using DFT calculations as presented in the methodology section. To ensure the accessibility of CH_3I into the hypothetical functionalized CAU-11-X series, MOFs whose pore limiting diameter (PLD) are smaller than 4.23 Å (the smallest Van der Waals diameter of CH_3I) are treated as inaccessible MOFs and excluded; a resulting eight CAU-11-X MOFs were obtained for further investigation (Figure 4b). Theoretical characterized porosity of the hypothetically designed MOFs and models of CH_3I-inaccessible CAU-11-X series are provided in the Section S7 of the Supporting Information. The adsorption isotherms of the four gases (CH_3I, CO_2, O_2, and N_2) up to 1 bar in the CAU-11-X MOFs were simulated by GCMC simulations and are given in Figure S22. Compared with CO_2, O_2, and N_2, CH_3I features a relatively larger molecular size, as shown in Figure S19, which contributes to an enhanced overlapped interaction between the gas molecules and the pore surface. As shown in Figure S22a, CH_3I adsorption isotherms of functionalized CAU-11-X series feature type I micropore filling adsorption mechanism, where the uptake can be saturated at relatively low pressure.

To elucidate the trace CH_3I separation performance of CAU-11-X series MOFs, we further studied the trace CH_3I separation performance under resembled nuclear industrial off-gas composition as the same conditions in the investigations of preliminary Al-MOFs. It appears that merely judging the CH_3I separation performance from adsorption isotherms up to 1 bar has provided false impression that postsynthetic modification is not working. As illustrated in Table 2, CAU-11-SO_3H gives the best performance in selectively capturing CH_3I by GCMC simulations (19.7 cm^3/g and 5.14 × 10^5), which is much higher than that of pristine CAU-11. The functionalization of CAU-11 has provided higher isosteric heat of adsorption (Q_{st}) of CH_3I with the MOFs with the exception of $-CH_3$ functionalization, which enabled higher CH_3I uptake, as shown in Figure 5a. The overall Q_{st} ranking is $-SO_3H$ > $-CN$ > $-NH_2$ > $-NO_2$ > $-Cl$ > $-Br$ > $-F$ > $-H$ > $-CH_3$, which fits well the CH_3I uptake ranking. The Q_{st} ranking from the GCMC simulations agrees well with the binding affinities obtained from DFT calculations, which confirms the validity of the GCMC simulation results. Moreover, as shown in Figure 5b, CH_3I selectivity ranking in the MOFs is positively correlated with the binding affinity differences between CH_3I and CO_2, N_2, and O_2. In general, CO_2 poses stronger

Table 2. CH_3I Separation Performance of the Functionalized CAU-11-X and Adsorption Affinity of the Adsorbates

CAU-11-X	CH_3I uptake (cm^3/g)	selectivity	E_{CH_3I}[a] (kJ/mol)	E_{CO_2} (kJ/mol)	E_{N_2} (kJ/mol)	E_{O_2} (kJ/mol)
$-SO_3H$	19.7	5.14 × 10^5	91.29	47.09	28.35	26.91
$-Br$	9.84	9.37 × 10^4	77.1	35.91	24.23	23.5
$-CH_3$	7.75	7.18 × 10^4	72.44	33.45	21.92	21.82
$-CN$	14.6	1.35 × 10^5	79.75	40.61	25.61	24.3
$-NO_2$	12.11	9.23 × 10^4	78.44	37.59	24.8	24.04
$-NH_2$	12.7	1.03 × 10^5	79.27	36.87	24.72	23.89
$-Cl$	11.95	9.58 × 10^4	77.34	36.03	24.12	23.38
$-F$	8.54	5.81 × 10^4	75.32	38.31	24.86	24.32
$-H$	11.18	6.64 × 10^4	71.9	32.85	21.87	21.04

[a]DFT-derived binding enthalpy.

https://doi.org/10.1021/acsomega.1c02072
ACS Omega 2021, 6, 18169−18177

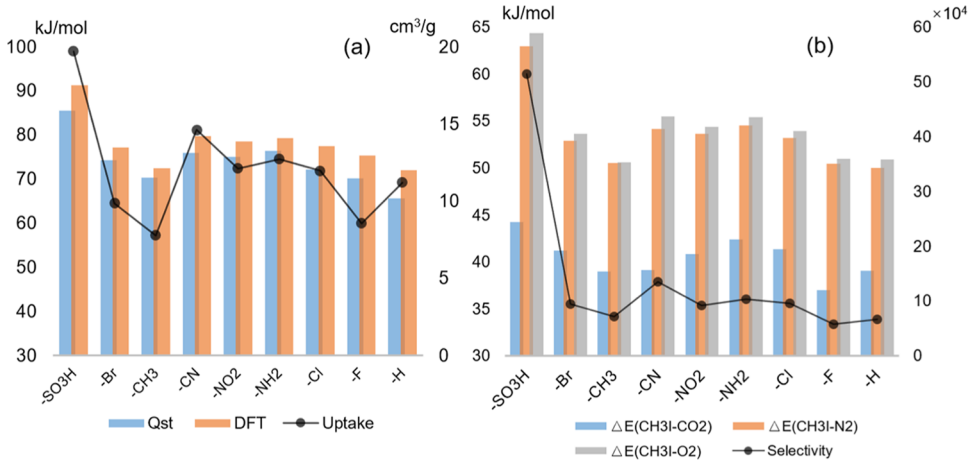

Figure 5. (a) Correlations between adsorption affinity and adsorption capacity of CH_3I in CAU-11-X series (blue bars stand for isosteric heat of adsorption calculated from GCMC simulation; orange bars stand for DFT-calculated adsorption enthalpy; and black dots stand for selectively adsorption capacity of CH_3I). (b) Correlations between adsorption enthalpy difference of CH_3I against other adsorbates and adsorption selectivity in CAU-11-X series (blue bars stand for adsorption enthalpy difference between CH_3I and CO_2; orange bars stand for adsorption enthalpy difference between CH_3I and N_2; gray bars stand for adsorption enthalpy difference between CH_3I and O_2; DFT-calculated adsorption enthalpy; and black dots stand for selectively adsorption selectivity of CH_3I).

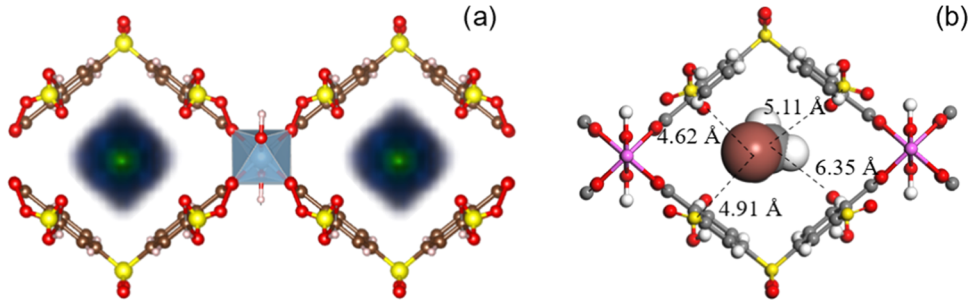

Figure 6. (a) Adsorption density plot pictures of CH_3I adsorbed in CAU-11-SO_3H during competitive adsorption. (b) DFT-optimized geometric positions of CH_3I in the CAU-11-SO_3H pore channel (color scheme: C, gray (brown in the density picture); H, white; O, red; Al, pink; and S, yellow).

adsorption competitiveness than N_2 and O_2 during the separation of CH_3I.

The adsorption enthalpy of CH_3I in CAU-11-SO_3H, at a close-to-saturation loading of 23.38 cc/g, was 85 kJ/mol, which is high for physisorption and could indicate difficulty in desorption. To evaluate the possibility of releasing CH_3I from CAU-11-SO_3H, we compared the zero-coverage isosteric heats of adsorption (Q_{st}) of CH_3I in CAU-11-SO_3H and HKUST-1(Cu), using the Widom particle insertion method. The zero-coverage Q_{st} is a direct measure of the adsorbent−adsorbate interaction strengths, which was calculated to be 77 and 67 kJ/mol for CH_3I in CAU-11-SO_3H and HKUST-1(Cu), respectively. In our calculations, any strong adsorbate interaction with the open metal sites of HKUST-1(Cu) was not captured beyond what was described by the used force field model for HKUST-1(Cu), which was a combination of UFF and DDEC charges. Therefore, the more accurate Q_{st} for HKUST-1(Cu) would be much higher than 67 kJ/mol should the strong adsorbate interactions with the open metal sites be included. Indeed, an appreciable percentage (5%) of adsorbed CH_3I in HKUST-1(Cu) was found to be from chemisorption; nonetheless, it was also shown that HKUST-1(Cu) exhibited a good adsorption/desorption cyclability.[11] Based on the relative adsorption strengths of CH_3I in CAU-11-SO_3H and HKUST-1(Cu), we envisage that the release of CH_3I from CAU-11-SO_3H might be possible.

Overall, we would like to propose CAU-11-SO_3H to be the best-performing trace CH_3I separation material, compared to other functionalization modifications, as it possesses the best CH_3I uptake and selectivity against (N_2, O_2, and CO_2) (19.7 cm^3/g and 5.14×10^5). However, the predicted adsorption capacity is not as high as the capacity measured for HKUST-1(Cu) by Chebbi et al.,[11] where breakthrough experiments were employed to investigate the dynamic adsorption properties of CH_3I in MOFs; see Table S19 for a comparison between CAU-11-SO_3H and selected MOFs from the literature. Different from breakthrough experiments, our GCMC simulations predict adsorption uptakes for a perfect crystalline structure, at a certain temperature and pressure, under thermodynamic equilibrium. By contrast, the dynamic adsorption in breakthrough experiments is additionally influenced by mesoscale factors, such as the height to the diameter ratio of the adsorbent bed and the flow conditions of the feed. It is also worth noting that the breakthrough experiments for HKUST-1(Cu) were conducted for 1333 ppm CH_3I with argon as a carrier gas, whereas we simulated for trace (100 ppm) CH_3I capture from a gas mixture also containing CO_2, N_2, and O_2.

https://doi.org/10.1021/acsomega.1c02072
ACS Omega 2021, 6, 18169−18177

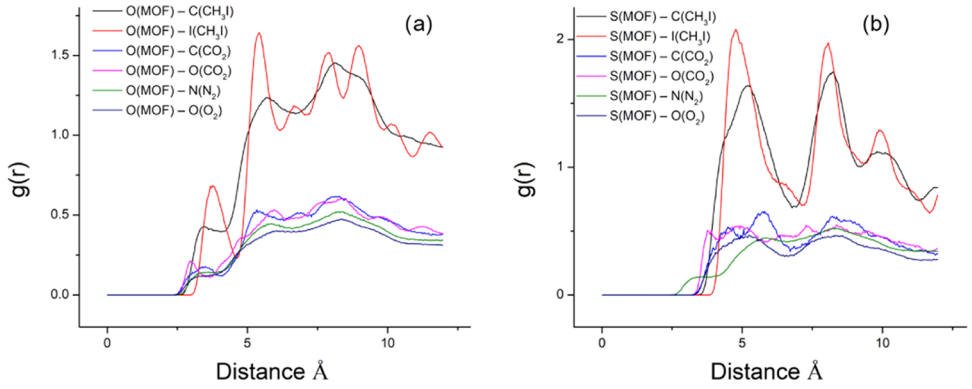

Figure 7. (a) Radial distribution functions of the O atoms of the SO_3H groups of CAU-11-SO_3H pairing various atoms of the adsorbates. (b) Radial distribution functions of the S atoms of the SO_3H groups of CAU-11-SO_3H pairing various atoms of the adsorbates (the C and I atoms were chosen for CH_3I).

To gain a molecular level of understanding of the competitive CH_3I adsorption behaviors in CAU-11-SO_3H, which proved to be the best adsorbent candidate in this study, a detailed investigation of adsorption sites and geometric positions of the adsorbates were carried out. Figure 6a presents the GCMC-simulated adsorption density plots of CH_3I molecules in CAU-11-SO_3H. CH_3I molecules are mainly located at the center of the pore channel. Due to the uniformly packed 1-D channel chain build up by SDBA-SO_3H and the induced joint effect by two polar centers provided by μ-OH groups and $-SO_2$, the density contour was lozenge shaped and seated parallel against the backbones of the framework. The DFT-optimized CH_3I binding position agrees well with the GCMC simulations results. It further reveals the sitting orientation of CH_3I in the channel. As shown in Figure 7b, the DFT-optimized CH_3I molecule is located in the center of the channel, where close distances of I···O and I···S are found to be 4.62 and 4.91 Å, respectively, indicating the favorable electrostatic interaction between the atom pairs. As with a less electron-dense site of the C center, the distances of C···S and C···O are 5.11 and 6.35 Å, respectively. The radial distribution analysis reveals that these atom pairs (I···O, I···S, C···S, and I···S) show clear regular peaks, indicating the regular sitting of CH_3I molecules along the pore channel of CAU-11-SO_3H. Such clear well-defined peaks are missing for N_2, O_2, and CO_2 adsorption in CAU-11-SO_3H, indicating their random sitting in the MOF.

CONCLUSIONS

To sum up, we have identified a promising Al-based MOF, CAU-11, for trace CH_3I capture, based on the combined GCMC- and DFT-calculated results. We demonstrated that the trace CH_3I separation performance could be enhanced by tuning the functionalization of the pore surface of CAU-11. The best-performing hypothetical CAU-11-SO_3H was proposed to possess both high selectivity and high adsorption capacity (19.7 cm^3/g and 5.14×10^5) in trace CH_3I capture, owing to the synergistic effect of the highly polarized functional group and good pore confinement. Since Al-based MOFs have been demonstrated to be highly radiation-resistant compared with MOF structures based on other metal types,[17] our work will provide good guidance on the design of materials that could be well applied in nuclear waste management.

COMPUTATIONAL DETAILS

Grand Canonical Monte Carlo Simulations. The RASPA package[32] was used to carry out the GCMC simulations of gas molecules' adsorption and separation in the MOFs. A typical GCMC simulation consists of an equilibrium run of 2×10^6 Monte Carlo (MC) cycles and a production run of 8×10^6 MC cycles. All of the MOF structures were kept rigid with periodic boundary conditions applied where the unit cell numbers were adjusted to ensure the perpendicular cell width to be longer than 24.0 Å (twice as the cutoff distance of 12.0 Å). The simulated gas composition was set to 100 ppm CH_3I, 400 ppm CO_2, 78% N_2, and 21% O_2 under 423 K, 1 bar. Such a system is intended to simulate a gaseous mixture released from the reprocessing of the spent nuclear fuel.[4,11] The selectivity of CH_3I in the simulated system is calculated by the following equation, where X_A and X_B are the mole fractions of targeted gas CH_3I and other gas components in the adsorbed phase, and Y_A and Y_B are the mole fractions of targeted gas CH_3I and other gas components in the bulk phase.

$$\text{selectivity}_{AB} = \frac{X_A/Y_A}{X_B/Y_B}$$

The structural properties, such as surface areas and porosity of the MOFs were characterized using the Zeo++ package.[33] To accurately address the electrostatic interaction, atomic charges of the structures were computed using the high-quality density-derived electrostatic charges (DDECs) method.[34] Lennard-Jones parameters of the adsorbents were taken from the universal force field.[35] Lorentz−Berthelot mixing rules were implemented to address the nonbonded interaction (Table 3).

Density Function Theory Calculations. DFT calculations were carried out using VASP[39−41] (Vienna Ab initio Simulation Package) with the plane-wave pseudopotential formalism. Geometric optimization of the MOFs and their binding complexes with the gas molecules were performed with the Perdew−Burke−Ernzerhof exchange−correlation functional.[42] DFT-D3(BJ) dispersion[43,44] correction was implemented to address the noncovalent bond interaction and the plane-wave cutoff energy was set to 500 eV.

The gas−MOF binding energies were calculated by the following equation

$$\Delta E = E_{bind} - E_{host} - E_{guest}$$

https://doi.org/10.1021/acsomega.1c02072
ACS Omega 2021, 6, 18169−18177

Table 3. Computational Model Parameters Governing Nonbonded Interactions

	atom label	ε/k_b (K)	σ (Å)
MOFs	Al	254.09	4.01
	C	52.83	3.43
	O	30.19	3.12
	H	51.22	3.40
	S	22.14	2.57
	N	34.72	3.26
	F	25.16	3
	Br	126.29	3.73
	Cl	114.21	3.52
adsorbates[36−38]	nitrogen_N	36.0	3.31
	methyl iodide_H	10.01	2.2.0
	methyl iodide_C	51.22	3.40
	methyl iodide_I	324.06	4.12
	carbon dioxide_O	79.0	3.05
	carbon dioxide_C	27.0	2.80
	oxygen_O	49.0	3.02

where E_{bind} is the zero-point energy of the optimized binding complex, E_{host} is the zero-point energy of the MOF cell, and E_{guest} is the zero-point energy of the guest gas molecules. During the DFT calculations, multiple initial positions of gas molecules were attempted to search for the global minimum interaction position of the gas molecules in the MOFs.

■ ASSOCIATED CONTENT

Supporting Information

The Supporting Information is available free of charge at https://pubs.acs.org/doi/10.1021/acsomega.1c02072.

The space-filling model of CAU-8-ODB; schematics of the asymmetric units of the Al-MOFs; schematics of the asymmetric units of CAU-11-X; models of the simulated gases; single-component adsorption isotherms of Al-MOFs; single-component adsorption isotherms of hypothetical CAU-11-X; calculated porosity properties of the CAU-11-X series; comparison between CAU-11-SO_3H and literature MOFs for capturing CH_3I; simulated adsorption and desorption of CH_3I in CAU-11-SO_3H; and potential synthetic routes for the grafted ligands (PDF)

Al-MOFs DDEC (ZIP)

CAU-11-X DDEC (ZIP)

■ AUTHOR INFORMATION

Corresponding Authors

Linjiang Chen − *Department of Chemistry and Materials Innovation Factory, University of Liverpool, Liverpool L7 3NY, United Kingdom; Leverhulme Research Centre for Functional Materials Design, Materials Innovation Factory and Department of Chemistry, University of Liverpool, Liverpool L7 3NY, United Kingdom*; Email: lchen@liverpool.ac.uk

Lifeng Ding − *Department of Chemistry, Xi'an JiaoTong-Liverpool University, Suzhou Dushu Lake Higher Education Town, Jiangsu 215123, China*; orcid.org/0000-0001-8761-191X; Email: Lifeng.Ding@xjtlu.edu.cn

Authors

Xiaoyu Wu − *Department of Chemistry, Xi'an JiaoTong-Liverpool University, Suzhou Dushu Lake Higher Education Town, Jiangsu 215123, China; Department of Chemistry and Materials Innovation Factory, University of Liverpool, Liverpool L7 3NY, United Kingdom*

Eric Jean Amigues − *Department of Chemistry, Xi'an JiaoTong-Liverpool University, Suzhou Dushu Lake Higher Education Town, Jiangsu 215123, China*

Ruiyao Wang − *Department of Chemistry, Xi'an JiaoTong-Liverpool University, Suzhou Dushu Lake Higher Education Town, Jiangsu 215123, China*

Zhongfu Pang − *Department of Chemistry and Materials Innovation Factory, University of Liverpool, Liverpool L7 3NY, United Kingdom; Leverhulme Research Centre for Functional Materials Design, Materials Innovation Factory and Department of Chemistry, University of Liverpool, Liverpool L7 3NY, United Kingdom*

Complete contact information is available at: https://pubs.acs.org/10.1021/acsomega.1c02072

Notes

The authors declare no competing financial interest.

■ ACKNOWLEDGMENTS

The authors acknowledge financial support from the Xi'an JiaoTong-Liverpool University Research Development Fund (RDF-16-02-03 and RDF-15-01-23) and the Key Program Special Fund (KSF-E-03). The authors acknowledge utilization of the computational resources from the Shenzhen Cloud Computing Center. L.C. and Z.P. acknowledge the Leverhulme Trust via the Leverhulme Research Centre for Functional Materials Design for funding. The authors thank Prof. Andrew Cooper for useful discussion.

■ REFERENCES

(1) Nandanwar, S. U.; Coldsnow, K.; Utgikar, V.; Sabharwall, P.; Eric Aston, D. Capture of Harmful Radioactive Contaminants from Off-Gas Stream Using Porous Solid Sorbents for Clean Environment − A Review. *Chem. Eng. J.* **2016**, 369−381.

(2) Adamantiades, A.; Kessides, I. Nuclear Power for Sustainable Development: Current Status and Future Prospects. *Energy Policy* **2009**, 5149−5166.

(3) Taghipour, F.; Evans, G. J. Radiolytic Organic Iodide Formation under Nuclear Reactor Accident Conditions. *Environ. Sci. Technol.* **2000**, *34*, 3012−3017.

(4) Bowyer, T. W.; Biegalski, S. R.; Cooper, M.; Eslinger, P. W.; Haas, D.; Hayes, J. C.; Miley, H. S.; Strom, D. J.; Woods, V. Elevated Radioxenon Detected Remotely Following the Fukushima Nuclear Accident. *J. Environ. Radioact.* **2011**, *102*, 681−687.

(5) Riley, B. J.; Vienna, J. D.; Strachan, D. M.; McCloy, J. S.; Jerden, J. L. Materials and Processes for the Effective Capture and Immobilization of Radioiodine: A Review. *J. Nucl. Mater.* **2016**, 307−326.

(6) Nenoff, T. M.; Rodriguez, M. A.; Soelberg, N. R.; Chapman, K. W. Silver-Mordenite for Radiologic Gas Capture from Complex Streams: Dual Catalytic CH3I Decomposition and I Confinement. *Microporous Mesoporous Mater.* **2014**, *200*, 297−303.

(7) Masson, O.; Baeza, A.; Bieringer, J.; Brudecki, K.; Bucci, S.; Cappai, M.; Carvalho, F. P.; Connan, O.; Cosma, C.; Dalheimer, A.; Didier, D.; Depuydt, G.; De Geer, L. E.; De Vismes, A.; Gini, L.; Groppi, F.; Gudnason, K.; Gurriaran, R.; Hainz, D.; Halldórsson, Ó.; Hammond, D.; Hanley, O.; Holeý, K.; Homoki, Z.; Ioannidou, A.; Isajenko, K.; Jankovic, M.; Katzlberger, C.; Kettunen, M.; Kierepko, R.; Kontro, R.; Kwakman, P. J. M.; Lecomte, M.; Leon Vintro, L.; Leppänen, A. P.; Lind, B.; Lujaniene, G.; Mc Ginnity, P.; Mahon, C. M.; Malá, H.; Manenti, S.; Manolopoulou, M.; Mattila, A.; Mauring, A.; Mietelski, J. W.; Møller, B.; Nielsen, S. P.; Nikolic, J.; Overwater,

R. M. W.; Pálsson, S. E.; Papastefanou, C.; Penev, I.; Pham, M. K.; Povinec, P. P.; Ramebäck, H.; Reis, M. C.; Ringer, W.; Rodriguez, A.; Rulík, P.; Saey, P. R. J.; Samsonov, V.; Schlosser, C.; Sgorbati, G.; Silobritiene, B. V.; Söderström, C.; Sogni, R.; Solier, L.; Sonck, M.; Steinhauser, G.; Steinkopff, T.; Steinmann, P.; Stoulos, S.; Sýkora, I.; Todorovic, D.; Tooloutalaie, N.; Tositti, L.; Tschiersch, J.; Ugron, A.; Vagena, E.; Vargas, A.; Wershofen, H.; Zhukova, O. Tracking of Airborne Radionuclides from the Damaged Fukushima Dai-Ichi Nuclear Reactors by European Networks. *Environ. Sci. Technol.* **2011**, *45*, 7670−7677.

(8) Gan, J.; Megonnell, N. E.; Yates, S. R. Adsorption and Catalytic Decomposition of Methyl Bromide and Methyl Iodide on Activated Carbons. *Atmos. Environ.* **2001**, *35*, 941−947.

(9) Park, S. W.; Lee, W. K.; Moon, H. Adsorption and Desorption of Gaseous Methyl Iodide in a Triethylenediamine-Impregnated Activated Carbon Bed. *Sep. Technol.* **1993**, *3*, 133−142.

(10) Haefner, D.; Tranter, T. Methods of Gas Phase Capture of Iodine from Fuel Reprocessing Off-Gas: A Literature Survey. *Idaho Natl. Lab.* 2007.

(11) Chebbi, M.; Azambre, B.; Volkringer, C.; Loiseau, T. Dynamic Sorption Properties of Metal-Organic Frameworks for the Capture of Methyl Iodide. *Microporous Mesoporous Mater.* **2018**, *259*, 244−254.

(12) Li, B.; Dong, X.; Wang, H.; Ma, D.; Tan, K.; Shi, Z.; Chabal, Y. J.; Han, Y.; Li, J. Functionalized Metal Organic Frameworks for Effective Capture of Radioactive Organic Iodides. *Faraday Discuss.* **2017**, *201*, 47−61.

(13) Li, B.; Dong, X.; Wang, H.; Ma, D.; Tan, K.; Jensen, S.; Deibert, B. J.; Butler, J.; Cure, J.; Shi, Z.; Thonhauser, T.; Chabal, Y. J.; Han, Y.; Li, J. Capture of Organic Iodides from Nuclear Waste by Metal-Organic Framework-Based Molecular Traps. *Nat. Commun.* **2017**, *8*, No. 485.

(14) Lan, Y.; Tong, M.; Yang, Q.; Zhong, C. Computational Screening of Covalent Organic Frameworks for the Capture of Radioactive Iodine and Methyl Iodide. *CrystEngComm* **2017**, *19*, 4920.

(15) Inl, T. *Forms Research and Development FY 2013 Accomplishments Report*, 2013.

(16) Lee, S. J.; Yoon, T. U.; Kim, A. R.; Kim, S. Y.; Cho, K. H.; Hwang, Y. K.; Yeon, J. W.; Bae, Y. S. Adsorptive Separation of Xenon/Krypton Mixtures Using a Zirconium-Based Metal-Organic Framework with High Hydrothermal and Radioactive Stabilities. *J. Hazard. Mater.* **2016**, *320*, 513−520.

(17) Volkringer, C.; Falaise, C.; Devaux, P.; Giovine, R.; Stevenson, V.; Pourpoint, F.; Lafon, O.; Osmond, M.; Jeanjacques, C.; Marcillaud, B.; Sabroux, J. C.; Loiseau, T. Stability of Metal-Organic Frameworks under Gamma Irradiation. *Chem. Commun.* **2016**, *52*, 12502−12505.

(18) Alvarez, E.; Guillou, N.; Martineau, C.; Bueken, B.; Vandevoorde, B.; Leguillouzer, C.; Fabry, P.; Nouar, F.; Taulelle, F.; Devos, D.; Chang, J. S.; Cho, K. H.; Ramsahye, N.; Devic, T.; Daturi, M.; Maurin, G.; Serre, C. The Structure of the Aluminum Fumarate Metal-Organic Framework A520. *Angew. Chem., Int. Ed.* **2015**, *54*, 3664−3668.

(19) Reinsch, H.; Feyand, M.; Ahnfeldt, T.; Stock, N. CAU-3: A New Family of Porous MOFs with a Novel Al-Based Brick: [Al 2(OCH 3) 4(O 2C-X-CO 2)] (X = Aryl). *Dalton Trans.* **2012**, *41*, 4164−4171.

(20) Reimer, N.; Reinsch, H.; Inge, A. K.; Stock, N. New Al-MOFs Based on Sulfonyldibenzoate Ions: A Rare Example of Intralayer Porosity. *Inorg. Chem.* **2015**, *54*, 492−501.

(21) Couck, S.; Liu, Y. Y.; Leus, K.; Baron, G. V.; Van Der Voort, P.; Denayer, J. F. M. Gas Phase Adsorption of Alkanes, Alkenes and Aromatics on the Sulfone-DUT-5 Metal Organic Framework. *Microporous Mesoporous Mater.* **2015**, *206*, 217−225.

(22) Godfrey, H. G. W.; da Silva, I.; Briggs, L.; Carter, J. H.; Morris, C. G.; Savage, M.; Easun, T. L.; Manuel, P.; Murray, C. A.; Tang, C. C.; Frogley, M. D.; Cinque, G.; Yang, S.; Schröder, M. Ammonia Storage by Reversible Host−Guest Site Exchange in a Robust Metal−Organic Framework. *Angew. Chem., Int. Ed.* **2018**, *57*, 14778−14781.

(23) Krüger, M.; Inge, A. K.; Reinsch, H.; Li, Y. H.; Wahiduzzaman, M.; Lin, C. H.; Wang, S. L.; Maurin, G.; Stock, N. Polymorphous Al-MOFs Based on V-Shaped Linker Molecules: Synthesis, Properties, and in Situ Investigation of Their Crystallization. *Inorg. Chem.* **2017**, *56*, 5851−5862.

(24) Loiseau, T.; Serre, C.; Huguenard, C.; Fink, G.; Taulelle, F.; Henry, M.; Bataille, T.; Férey, G. A Rationale for the Large Breathing of the Porous Aluminum Terephthalate (MIL-53) Upon Hydration. *Chem. - Eur. J.* **2004**, *10*, 1373−1382.

(25) Assfour, B.; Assaad, T.; Odeh, A. In Silico Screening of Metal Organic Framework for Iodine Capture and Storage. *Chem. Phys. Lett.* **2014**, *610*−*611*, 45−49.

(26) Mohideen, M. I. H.; Pillai, R. S.; Adil, K.; Bhatt, P. M.; Belmabkhout, Y.; Shkurenko, A.; Maurin, G.; Eddaoudi, M. A Fine-Tuned MOF for Gas and Vapor Separation: A Multipurpose Adsorbent for Acid Gas Removal, Dehydration, and BTX Sieving. *Chem* **2017**, *3*, 822−833.

(27) Qiao, Z.; Xu, Q.; Jiang, J. High-Throughput Computational Screening of Metal-Organic Framework Membranes for Upgrading of Natural Gas. *J. Membr. Sci.* **2018**, *551*, 47−54.

(28) Maity, R.; Singh, H. D.; Yadav, A. K.; Chakraborty, D.; Vaidhyanathan, R. Water-Stable Adenine-Based MOFs with Polar Pores for Selective CO2 Capture. *Chem. - Asian J.* **2019**, *14*, 3736−3741.

(29) Li, H.; Wang, K.; Hu, Z.; Chen, Y. P.; Verdegaal, W.; Zhao, D.; Zhou, H. C. Harnessing Solvent Effects to Integrate Alkylamine into Metal-Organic Frameworks for Exceptionally High CO2 Uptake. *J. Mater. Chem. A* **2019**, *7*, 7867−7874.

(30) Zeng, X. Y.; Wang, Y. L.; Lin, Z. T.; Liu, Q. Y. Proton-Conductive Coordination Polymers Based on Diphenylsulfone-3,3′-Disulfo-4,4′-Dicarboxylate with Well-Defined Hydrogen Bonding Networks. *Inorg. Chem.* **2020**, *59*, 12314−12321.

(31) Qin, S.; Zhang, P.; Qin, Y. J.; Guo, Z. X. Facile Synthesis of Diarylsulfones from Arenes and 3CdSO4·xH2O via Mechanochemistry. *Tetrahedron Lett.* **2020**, *61*, No. 151567.

(32) Dubbeldam, D.; Calero, S.; Ellis, D. E.; Snurr, R. Q. RASPA: Molecular Simulation Software for Adsorption and Diffusion in Flexible Nanoporous Materials. *Mol. Simul.* **2016**, *42*, 81−101.

(33) Willems, T. F.; Rycroft, C. H.; Kazi, M.; Meza, J. C.; Haranczyk, M. Algorithms and Tools for High-Throughput Geometry-Based Analysis of Crystalline Porous Materials. *Microporous Mesoporous Mater.* **2012**, *149*, 134−141.

(34) Manz, T. A.; Sholl, D. S. Chemically Meaningful Atomic Charges That Reproduce the Electrostatic Potential in Periodic and Nonperiodic Materials. *J. Chem. Theory Comput.* **2010**, *6*, 2455−2468.

(35) Rappé, A. K.; Casewit, C. J.; Colwell, K. S.; Goddard, W. A.; Skiff, W. M. UFF, a Full Periodic Table Force Field for Molecular Mechanics and Molecular Dynamics Simulations. *J. Am. Chem. Soc.* **1992**, *114*, 10024−10035.

(36) Yuan, Y.; Dong, X.; Chen, Y.; Zhang, M. Computational Screening of Iodine Uptake in Zeolitic Imidazolate Frameworks in a Water-Containing System. *Phys. Chem. Chem. Phys.* **2016**, *18*, 23246−23256.

(37) Ge, Y.; Zhou, H.; Ji, Y.; Ding, L.; Cheng, Y.; Wang, R.; Yang, S.; Liu, Y.; Wu, X.; Li, Y. Understanding Water Adsorption and the Impact on CO2 Capture in Chemically Stable Covalent Organic Frameworks. *J. Phys. Chem. C* **2018**, *122*, 27495−27506.

(38) Moghadam, P. Z.; Islamoglu, T.; Goswami, S.; Exley, J.; Fantham, M.; Kaminski, C. F.; Snurr, R. Q.; Farha, O. K.; Fairen-Jimenez, D. Computer-Aided Discovery of a Metal-Organic Framework with Superior Oxygen Uptake. *Nat. Commun.* **2018**, *9*, No. 1378.

(39) Kresse, G. Ab Initio Molecular Dynamics for Liquid Metals. *J. Non-Cryst. Solids* **1995**, *192*−*193*, 222.

(40) Kresse, G.; Furthmüller, J. Efficient Iterative Schemes for Ab Initio Total-Energy Calculations Using a Plane-Wave Basis Set. *Phys. Rev. B* **1996**, *54*, 11169−11186.

(41) Kresse, G.; Furthmüller, J. Software VASP, Vienna. *Phys. Rev. B* **1996**, *54*, 11169.

https://doi.org/10.1021/acsomega.1c02072
ACS Omega 2021, 6, 18169−18177

(42) Perdew, J. P.; Burke, K.; Ernzerhof, M. Generalized Gradient Approximation Made Simple. *Phys. Rev. Lett.* **1996**, *77*, 3865.
(43) Grimme, S.; Antony, J.; Ehrlich, S.; Krieg, H. A Consistent and Accurate Ab Initio Parametrization of Density Functional Dispersion Correction (DFT-D) for the 94 Elements H-Pu. *J. Chem. Phys.* **2010**, *132*, No. 154104.
(44) Grimme, S.; Ehrlich, S.; Goerigk, L. Effect of the Damping Function in Dispersion Corrected Density Functional Theory. *J. Comput. Chem.* **2011**, *32*, 1456−1465.

https://doi.org/10.1021/acsomega.1c02072
ACS Omega 2021, 6, 18169−18177